Gating charge displacement in a monomeric voltage-gated proton (H_v1) channel

Emerson M. Carmona[a], H. Peter Larsson[b], Alan Neely[a], Osvaldo Alvarez[a,c], Ramon Latorre[a,1], and Carlos Gonzalez[a,1]

[a]Centro Interdisciplinario de Neurociencia de Valparaíso, Universidad de Valparaíso, 2351319 Valparaíso, Chile; [b]Department of Physiology and Biophysics, University of Miami, Miami, FL 33136; and [c]Departamento de Biología, Facultad de Ciencias, Universidad de Chile, 7800003 Santiago, Chile

Contributed by Ramon Latorre, July 18, 2018 (sent for review June 6, 2018; reviewed by Thomas E. DeCoursey and Francesco Tombola)

The voltage-gated proton (H_v1) channel, a voltage sensor and a conductive pore contained in one structural module, plays important roles in many physiological processes. Voltage sensor movements can be directly detected by measuring gating currents, and a detailed characterization of H_v1 charge displacements during channel activation can help to understand the function of this channel. We succeeded in detecting gating currents in the monomeric form of the *Ciona*-H_v1 channel. To decrease proton currents and better separate gating currents from ion currents, we used the low-conducting H_v1 mutant N264R. Isolated ON-gating currents decayed at increasing rates with increasing membrane depolarization, and the amount of gating charges displaced saturates at high voltages. These are two hallmarks of currents arising from the movement of charged elements within the boundaries of the cell membrane. The kinetic analysis of gating currents revealed a complex time course of the ON-gating current characterized by two peaks and a marked Cole–Moore effect. Both features argue that the voltage sensor undergoes several voltage-dependent conformational changes during activation. However, most of the charge is displaced in a single central transition. Upon voltage sensor activation, the charge is trapped, and only a fast component that carries a small percentage of the total charge is observed in the OFF. We hypothesize that trapping is due to the presence of the arginine side chain in position 264, which acts as a blocking ion. We conclude that the movement of the voltage sensor must proceed through at least five states to account for our experimental data satisfactorily.

Hv1 proton channel | gating currents | trapping | voltage sensor | kinetic model

Voltage-gated proton (H_v1) channels are transmembrane proteins that regulate cellular pH, producing outward proton currents in response to depolarization. Since the discovery of the *Ciona intestinalis*, mouse, and human H_v1 genes in 2006 (1, 2), the relevance of this channel in physiological and pathophysiological processes has increased continuously (3). H_v1 is a voltage-gated ion channel with a unique structure and properties. It is a homodimer (4–6) containing four transmembrane alpha helixes in each subunit (S1 to S4). Both the voltage sensor and the permeation pathway of this channel originate from these four transmembrane segments. The fourth transmembrane helix (S4) contains three conserved arginine residues responsible for the channel voltage sensitivity (7, 8) The intracellular N-terminal domain is variable in both length and sequence among different species. The intracellular C-terminal domain forms a coiled-coil structure necessary for dimer formation (6). H_v1 is voltage- (7) and pH-dependent (9), is highly selective to protons (10), has a small unitary conductance (11), and displays a cooperative gating between subunits (8, 12). However, there are still many open questions regarding the mechanisms of H_v1 activation. In particular, we do not know the details regarding how the gating charges are displaced during activation and how these movements are related to channel opening.

H_v1 voltage sensor movement has been studied principally by two methods: accessibility assays and fluorescence. In the first case, membrane-impermeable thiol-reactive methanethiosulfonate (MTS) probes were used to test the state-dependent accessibility of a cysteine residue introduced into a specific region of the voltage sensor (13). In the case of H_v1, accessibility experiments indicate that both S1 (14) and S4 (7) undergo conformational changes during activation and that there is cooperativity between the subunits of the channel (8). The second approach involves the use of voltage-clamp fluorometry (VCF) (15). In VCF, the conformational changes of the channel are monitored by a fluorescent probe bound to a cysteine introduced into a specific site using mutagenesis (16, 17). VCF experiments revealed two conformational changes during activation (18); following the S4 movement, there is a displacement of S1 associated with the opening of the channel (14). The caveat of these methodologies is that they are indirect approaches to studying the dynamics of the H_v1 voltage sensor. In contrast, gating currents directly report the movement of the voltage-sensing charges across the membrane electric field, making it possible to study the kinetics of this process in detail.

In the *Shaker* voltage-gated potassium channel, gating currents are produced by the movement of arginine residues in the S4 transmembrane segment within the voltage sensor domain (19, 20). Three of these arginine residues are conserved in S4 of H_v1 and were shown to be responsible for the voltage-dependent gating of the channel (7). Since the *Ciona*-H_v1 channels express well in oocytes, it should be possible to record gating currents induced by the activation of this channel. Indeed, preliminary studies on H_v1 gating current have been reported (21–23).

Significance

H_v1 proton channels, since their open probability increases with depolarization and low pH, are fundamental in sustaining the suitable pH gradient for cell survival. Here, we have characterized the gating current elicited by the monomeric mutant proton channel N264R with the aim of understanding the voltage-dependent processes that control channel opening. Gating currents precede ion currents, indicating that a large fraction of gating charge is displaced before H_v1 opening. The voltage sensor displacements are complex and consist of numerous well-defined states. However, most of the charge is displaced in a single transition that probably leads to channel opening. The positively charged arginine in the N264R channel promotes gating charge trapping in addition to blocking the proton currents.

Author contributions: E.M.C., H.P.L., A.N., O.A., R.L., and C.G. designed research; E.M.C. performed research; E.M.C., H.P.L., A.N., O.A., R.L., and C.G. analyzed data; and E.M.C., H.P.L., A.N., O.A., R.L., and C.G. wrote the paper.

Reviewers: T.E.D., Rush University; and F.T., University of California, Irvine.

The authors declare no conflict of interest.

See Commentary on page 9057.

[1]To whom correspondence may be addressed. Email: ramon.latorre@uv.cl or carlos.gonzalezl@uv.cl.

This article contains supporting information online at www.pnas.org/lookup/suppl/doi:10.1073/pnas.1809705115/-/DCSupplemental.

Published online August 20, 2018.

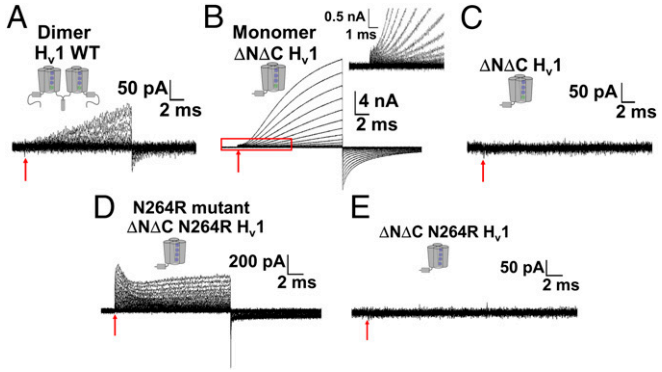

Fig. 1. An early nonlinear capacitive current was detected in the monomeric H_v1. (*A*) Currents produced by the dimeric H_v1 did not show an initial nonlinear capacitive component. (*B*) Currents produced by the monomeric form of the channel presented an initial step (*Inset*) preceding the development of fast proton currents. (*C*) A hyperpolarizing protocol applied to patches expressing the monomeric H_v1 did not produce similar currents. (*D*) Currents produced by the conductance-impaired monomeric H_v1 mutant N264R presented an initial nonlinear transient current followed by the development of proton currents. (*E*) A hyperpolarizing protocol applied to patches expressing the monomeric H_v1 mutant N264R did not produce currents. Superimposed current traces were recorded for membrane voltage steps from −90 to 200 mV in 10-mV increments in *A* and *B*, from −90 to 260 mV in 10-mV increments in *D*, and from −330 to −50 mV in 10-mV increments in *C* and *E*. Red arrows indicate the time at which the voltage pulses were applied. Holding potential was −70 mV. Linear capacitive current was subtracted online using a P/-8 pulse protocol.

Results

H_v1 Gating Currents Are Revealed in Monomeric Channels and Better Resolved in Conductance-Impaired N264R Mutant. To detect H_v1 gating currents, we expressed *C. intestinalis* H_v1 channels in *Xenopus laevis* oocytes and recorded membrane currents in giant patches (inside-out configuration and symmetrical pH = 7.0). In dimeric H_v1, we were unable to resolve any initial transient current consistent with nonlinear capacitive currents. At short times after the onset of the depolarizing pulse, we observed a monotonic development of current free of any transient component (Fig. 1*A*). In contrast, upon depolarization, oocyte membrane patches expressing fast activating monomeric channels displayed an initial current transient that preceded the development of ion currents (Fig. 1*B*). As expected for gating currents, these initial transient currents were absent during hyperpolarizing pulses (Fig. 1*C*). We conclude that our failure to detect gating currents in the dimeric H_v1 channels was because of their slow kinetics and small amplitude.

Since ion currents heavily contaminate the putative gating currents from monomeric H_v1, we resorted to the N264R mutant of monomeric H_v1 that greatly decreases proton currents while retaining voltage sensor movement as assayed by indirect methods (18, 24). At depolarizing voltages, currents recorded from this mutant channel showed an early transient current followed by increasing outward currents (Fig. 1*D*). During repolarization, we could distinguish a rapid transient current, followed by a nearly constant component. Most likely, the transient component is gating charge movement, and the slow component is a mix of ion and gating current (Fig. 1*D*). To corroborate that the ON-transient was due to nonlinear charge movement, we also show that hyperpolarization-evoked currents lack this component (Fig. 1*E*). The following analysis will demonstrate that the early currents in Fig. 1*D* are indeed gating currents.

H_v1 Gating Currents Can Be Isolated from Ion Currents. Isolation of the ON-gating currents was performed numerically, assuming that the currents recorded from monomeric H_v1 mutant (I_{exp}) were the sum of gating (I_g) and ion currents (I_i) (21):

$$I_{exp}(t) = I_g(t) + I_i(t). \quad [1]$$

Gating currents were modeled as a product of an increasing and a decreasing exponential function, corresponding to the rising and decaying phase of the gating currents, respectively:

$$I_g(t) = A\left(1 - e^{-t/\tau_1}\right)e^{-t/\tau_2}, \quad [2]$$

where A is the amplitude and τ_1 and τ_2 are the time constants of the increasing and the decreasing exponential functions, respectively. Ion currents were modeled as an exponential function raised to the power of two with a time constant τ_3, that accounts for the sigmoidal shape of macroscopic current time course from mutant monomeric H_v1 (Fig. 1*B*):

$$I_i(t) = B\left(1 - e^{-t/\tau_3}\right)^2, \quad [3]$$

where B is the amplitude of the ion current component. Fig. 2*A* shows examples of the fitting procedure of the current records at six different voltages. Plots of the isolated gating currents $I_g(t)$ show that both the amplitude and the rate of decay increase with voltage as expected from bona fide gating currents (Fig. 2*B*). The time course of the charge displaced, obtained by integrating $I_g(t)$, is shown in Fig. 2*C*. The time constant of the gating current decay (τ_2) (Eq. **2**) vs. voltage data was fitted assuming that the conformational change of the voltage sensor is well-described by a first-order process: resting-active (A-B) (Fig. 2*D*, open circles). In the A-B two-state model, voltage-dependent time constants and rates are given by the equations

$$\tau(V) = \frac{1}{\alpha(V) + \beta(V)}, \alpha(V) = \alpha_0 e^{\frac{z\delta_\alpha e_0 V}{kT}}, \beta(V) = \beta_0 e^{\frac{-z\delta_\beta e_0 V}{kT}}, \quad [4]$$

where α(V) and β(V) are the forward and backward rates, respectively, and α_0 and β_0 are the rate constants for $V = 0$ mV, $z\delta_\alpha$

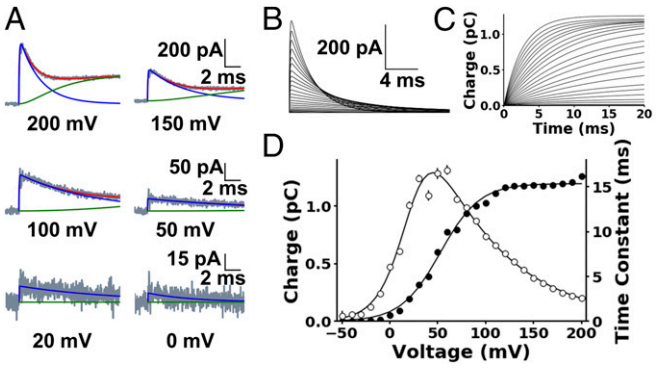

Fig. 2. Isolated ON-gating currents were voltage-dependent. (*A*) Representative experimental currents recorded for the monomeric H_v1 mutant N264R during depolarizations at the indicated voltages (I_{exp}, black traces). They were fitted with Eq. **1** to isolate the ON-gating current (I_g, blue traces) from the ion current (I_i, green traces). Holding potential was −70 mV. (*B*) Superimposed plots of the isolated ON-gating currents for membrane voltage steps from −90 to 200 mV in 10-mV increments. (*C*) Time course of the gating charge displaced obtained integrating the gating currents shown in *B*. (*D*) Time constants of the I_g decay (open circles) and charge displaced as function of voltage [$Q(V)$ curve, filled circles]. Time constant data were fitted using a two-state model (solid line), where $\alpha_0 = 0.027 \pm 0.002$ ms^{-1}, $\beta_0 = 1.53 \pm 0.01$ ms^{-1}, $z\delta_\alpha = 0.34 \pm 0.02$, and $z\delta_\beta = 1.44 \pm 0.12$. The $Q(V)$ curve was fitted by a Boltzmann function (solid line, Eq. **5**), where $V_{0.5} = 52.8 \pm 1.1$ mV and $z\delta = 1.23 \pm 0.06$. Error bars are the SD of the parameters obtained in the fitting procedure. The average values of the $Q(V)$ parameters ($n = 10$) were as follows: $z\delta = 1.05 \pm 0.09$ and $V_{0.5} = 54.8 \pm 7.9$ mV.

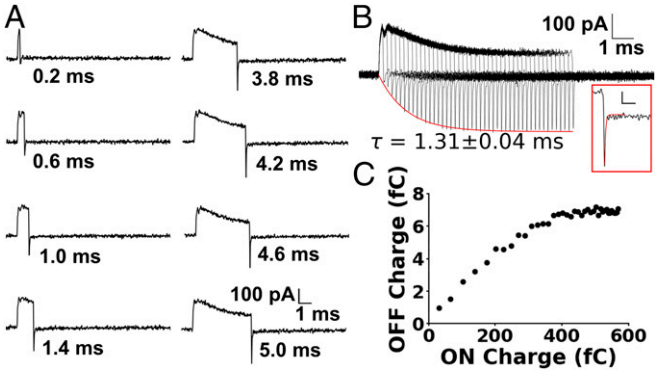

Fig. 3. Gating charge is trapped during voltage sensor activation. (*A*) Currents recorded for a series of depolarizations with different durations. The protocol consisted of a prepulse voltage of −70 mV, followed by a test pulse to 150 mV and repolarization to 0 mV (reversal potential). Depolarization was imposed during the time indicated for each trace. (*B*) Superimposed series of current records produced by short depolarizations from a prepulse voltage of −70 mV, depolarization to 150 mV, and a repolarization to 0 mV. Each trace is separated from the following by a 0.2-ms time increment. The time course of the fast component is described by the red line. (*Inset*) OFF-gating current is well-described by a single exponential of 0.03 ms (red trace). (Scale bars: 50 pA and 0.4 ms.) (*C*) OFF-gating charge as a function of the ON-gating charge for pulses of different durations. OFF charge was calculated multiplying the amplitude of the current by the time constant of decay (0.03 ms) while ON charge was integrated numerically, using the time constant at 150 mV (see text).

and $z\delta_\beta$ describe the voltage dependence of the rates, e_0 is the elementary charge, and k and T have their usual meanings. The parameters that best described the data shown were $\alpha_0 = 0.027 \pm 0.002$ ms^{-1}, $\beta_0 = 1.53 \pm 0.01$ ms^{-1}, $z\delta_\alpha = 0.34 \pm 0.02$, and $z\delta_\beta = 1.44 \pm 0.12$ (Fig. 2*D*, solid line). β(V) is more voltage-dependent than α(V), and, as a result, the bell-shaped time constant vs. voltage plot is asymmetric (Fig. 2*D*).

Charge displaced at each voltage was obtained from the area under the corresponding isolated gating current: i.e., A times τ_2, (Eq. **2** and Fig. 2*D*, filled circles). This $Q(V)$ curve showed a voltage-dependent saturation and was well-fitted using a Boltzmann function:

$$Q(V) = \frac{Q_{max}}{1 + e^{\frac{-z\delta e_0 (V - V_{0.5})}{kT}}}, \qquad [5]$$

with half-activation voltage ($V_{0.5}$) of 52.8 ± 1.1 mV and effective valence ($z\delta$) of 1.23 ± 0.06 (Fig. 2*D*, solid line). For a set of 10 independent experiments, the average values of the parameters were as follows: $z\delta = 1.05 \pm 0.09$ and $V_{0.5} = 54.8 \pm 7.9$ mV (mean ± SEM).

H_v1 Gating Current Kinetics Revealed That a Large Fraction of the Charge Is Trapped. Fig. 2*A* shows that gating currents precede the development of ion currents, giving us a time window to characterize them in more detail. Accordingly, to minimize the activation of ion currents, we measured the OFF-gating currents after very short depolarizations. Furthermore, after the pulse to 150 mV, the membrane potential was returned to the reversal potential of the proton currents (0 mV). Upon returning to 0 mV, we observed a rapid transient with a 0.03-ms time constant (Fig. 3 *A* and *B*, *Inset*). However, the OFF-gating charges displaced during these brief transients were only a minute fraction of that displaced during the ON. This discrepancy indicates that, while dwelling at 150 mV, a large fraction of the charges became trapped in a deep well. The amplitude of the OFF-gating currents increased with the duration of the depolarizing pulse and reached a plateau following an exponential function with a time constant of 1.31 ± 0.04 ms. (Fig. 3*B*). We computed the charge of OFF transient by multiplying the amplitude of the transient by the decay time constant of the spike (τ = 0.03 ms). The time course of the ON-gating current cannot be calculated directly from the current records due to the ion current contamination. To calculate the ON-gating charge, we integrated the current numerically from the beginning of the depolarizing pulse up to 1 ms. From 1 ms on, we integrated the rest of the charge by multiplying the amplitude of the current at 1 ms by the 4-ms time constant of the gating current decay at 150 mV (Fig. 2*D*). With these ON and OFF charges, we built the graph shown in Fig. 3*C*. For long depolarizing pulses, the OFF/ON charge ratio was 7/500 (or 1.4% of the ON).

Trapped H_v1 Gating Charge Is Recovered During Repolarization. We next designed a protocol to recover the ON-gating charges, consisting of two 20-ms depolarization pulses to 150 mV from a holding potential of −70 mV, separated by a sojourn of increasing duration at −70 mV (Fig. 4 *A* and *B*). If the trapped gating charge returns slowly at −70 mV, the recovered charge can be measured during the second depolarizing pulse. At the onset of the second depolarization, a brief spike was recorded, followed by a pedestal of ion current. The spike only appeared after a brief repolarization period: e.g., 2 ms. This ON spike is the mirror image of the OFF spike seen at the onset of the preceding repolarization. With a longer sojourn at −70 mV (50 ms), the ON spike disappeared, and the gating current reached an amplitude comparable with that of the first 20-ms pulse (Fig. 4 *A* and *B*). The origin of the OFF and ON spikes will be explained with a five-state kinetic model (see below). The amount of charge recovered during the second pulse increased following an exponential time course with a time constant of 87.6 ± 7.4 ms (Fig. 4 *B* and *C*). The charge extrapolated at very long times, Q_∞, was 1,566 ± 80 fC (Fig. 4*C*), which compares

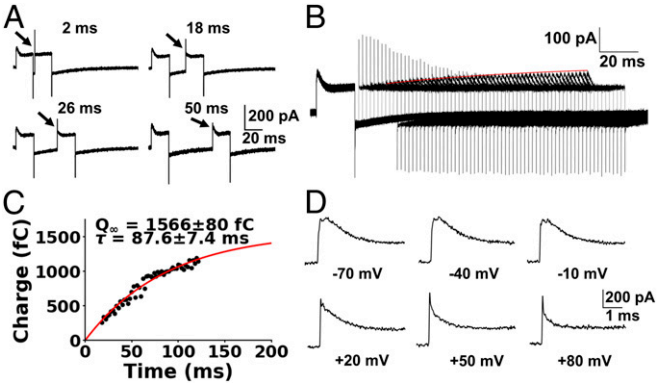

Fig. 4. The OFF-gating charge is recovered slowly. (*A*) ON-gating current recovery protocol for four different times. Two depolarizing pulses from a holding potential of −70 mV to 150 mV were separated by the time indicated. A fast outward gating current appeared at short intervals, and it decreased at longer intervals, while a second slower component appeared at longer intervals (arrows). (*B*) Superimposed currents produced by the ON recovery protocol from a holding potential of −70 mV and depolarization to 150 mV. The interval of time between the depolarizing pulses increased 2 ms between traces. The red line describes the time course of the ON-gating charge recovery. (*C*) The charge displaced during the slow component of the second depolarization as a function of the time interval between the depolarizations. The data were fitted using a single increasing exponential function $Q_\infty[1 - \exp(-t/\tau)]$ where Q_∞ is the exponential amplitude and τ is the time constant. Note that the asymptote of the curve is 1,566 ± 80 fC, meaning that the charge is recovered completely. (*D*) Cole–Moore effect of the ON-gating current when a depolarizing pulse of 200 mV is preceded by the prepulse voltage indicated. Note how the two peaks of current are converted into a single peak of current and the kinetics of decay gets faster as the prepulse voltage becomes more positive.

well with the charge displaced during the ON (1,500 fC). Note that the fast transient current during the ON-gating currents was only present when the repolarization period was short and disappeared at long repolarizations (Fig. 4 *A* and *B*). Moreover, we had consistently observed two peaks and a rising phase in the ON-gating current at 150 mV, when the holding voltages were sufficiently negative (negative voltages in Figs. 3*A* and 4*D*). However, when we increased the holding voltages, only a single peak was detected (positive voltages in Fig. 4*D*). The rate of decay of the gating currents was also affected by the initial conditions, being faster with prepulse voltages above 0 mV (*SI Appendix*, Fig. S1 *A* and *B*). This protocol is equivalent to the well-known Cole–Moore effect (25, 26) and can reveal that the voltage sensor undergoes multiple voltage-dependent transition states (*Discussion*) preceding the voltage sensor activation and channel opening (*SI Appendix*, Fig. S1 *C* and *D*). A Cole–Moore shift in dimeric native H_v1 channels has been reported previously (27). However, our results show that this effect is also present in the monomeric form of the channel, indicating that the monomer also transits through several closed states before channel opening.

Discussion

Gating Current Measurements. The two main difficulties for measuring gating currents in the WT dimeric H_v1 are the slow kinetics of activation (*SI Appendix*, Figs. S2*A* and S3), which possibly is correlated with a slow movement of the voltage sensor, and the inability to eliminate or reduce significantly proton currents through the channels. Here, we used an experimental strategy that enabled us to detect and characterize the H_v1 charge displacement. Since the kinetics of proton currents in the monomeric form of the channel develop much faster than those in the dimer (*SI Appendix*, Figs. S2 and S3), implying a faster increase in the H_v1 voltage-dependent open probability, we expected to find gating currents faster and with larger amplitudes. Also, to minimize the proton currents, we used the monomeric low-conducting mutant N264R (*SI Appendix*, Figs. S2*C* and S3). Notably, the N264R mutant has almost the same voltage dependence as the WT form of H_v1 (*SI Appendix*, Figs. S3 and S4).

Gating currents must obey certain rules demanded by the confined space in which they move. First, the charge versus voltage (Q-V) curve should saturate at high voltages at which all voltage sensors are activated. Second, gating currents should become larger and faster as the voltage is increased: i.e., the gating current kinetics is voltage-dependent (28). Third, all of the charge displaced during the ON must be recovered during the OFF. In the N264R mutant, we isolated the gating currents analytically, and the resulting nonlinear currents displayed kinetics and voltage dependence that satisfied the first two criteria. However, the OFF represented only 1.4% of the ON-gating charges. This phenomenon reminded us of charge immobilization first reported for the sodium channel (29). Here, we prefer to use the concept of trapping since modeling of the gating kinetics data suggests that, upon activation, charge needs to surmount a large barrier to return to its initial configuration (see below).

A Two-State Model Is Not Enough to Recapitulate Gating Charge Displacement in H_v1 Channels. To analyze isolated gating currents, we assumed a two-state model: resting (A)–active (B). However, a closer inspection of the data suggests that the movement of the voltage sensor in monomeric H_v1 is more complex than a two-state process. The first observation that caught our attention was the fact that only a very small fraction of the ON-gating charge was recovered in the OFF (Fig. 3*C*), suggesting that the return of the charge to the resting state is very slow indeed. Actually, the double pulse experiments of Fig. 4 suggest that, to return to the resting state, the voltage sensor needs to undergo at least two transitions: $A \leftrightarrow B_1 \leftrightarrow B_2$, where A is the resting state, and that a large energy barrier separates states A from B_1. The fast transition seen in the OFF is determined by the B_2-to-B_1 transition, and the slow charge return, defined by the 88-ms time constant (Fig. 4*C*), represents the transition from B_1 to A. However, the presence of two peaks in the ON-gating current and the pronounced Cole–Moore effect also suggest that, to reach state B_1, the voltage sensor undergoes first a fast transition defining the first peak A_1-A_2 and a slower transition A_2-A_3 before reaching the B_1 state. Therefore, charge trapping is a consequence of the large energy barrier separating states A_3 from B_1 (see below). Against a two-state model is also the fact that the Boltzmann describing the Q-V curve yields a $z\delta$ close to 1 (Fig. 2), in contrast to the limiting slope experiments that set a lower limit to near three gating charges per monomeric H_v1 channel (8). This discrepancy suggests that there is more than one step involved in the voltage sensor activation (30).

A Five-State Model Reproduced H_v1 Gating Current Features. Taking into account all of the results presented, we propose a sequential model for the movement of the monomeric H_v1 voltage sensor consisting of five states (A_1, A_2, A_3, B_1, and B_2) separated by four transitions (Fig. 5*A* and *SI Appendix*, Fig. S5). States A_1 to A_3 are revealed during H_v1 channel activation (Fig. 4*D* and *SI Appendix*, Fig. S1), and B_1 and B_2 during channel deactivation (Fig. 4 *A* and *B*). Gating currents simulated from our five-state model presented two peaks of currents in the ON and only a fast component in the OFF (Fig. 5*B*), reproducing the experimental currents. Additionally, it can reproduce the transients observed during activation and deactivation and the Cole–Moore effect at different prepulse voltages (Fig. 5 *C*–*E*). Our model shows that the kinetics of the ON-gating current is dominated by the highest energy barrier placed between A_3 and B_1 (32 kJ/mol). Application of a 150-mV

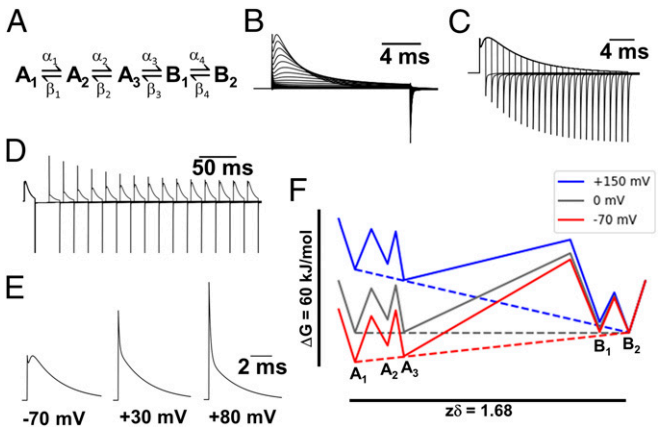

Fig. 5. A five-state model can reproduce the features of the H_v1 gating currents. (*A*) Five-state sequential model used to simulate H_v1 gating currents. Rates and voltage dependence of each transition are given in *SI Appendix*, Table S1. (*B*) Superimposed simulated traces of gating currents produced by the model. A prepulse at −70 mV was followed by a series of voltage steps from −90 to 200 mV in 10-mV increments and repolarization to 0 mV. Note the presence of two peaks during the ON-gating current and the large difference between the gating charge displaced during the ON and OFF components. (*C*) Superimposed simulated traces of depolarizations at 150 mV of increasing duration produced a fast OFF component that increases at short depolarizations to reach a plateau during repolarization at 0 mV, similar to Fig. 3*B*. Holding potential is −70 mV, and the time interval of depolarization increased 1 ms between current traces. (*D*) Superimposed simulated traces of the ON recovery protocol similar to the protocol of Fig. 4*B*. Holding potential is −70 mV, and depolarizations were produced at 150 mV. The time interval between depolarizations increases 20 ms between traces. (*E*) Simulated traces of the ON-gating current produced with a depolarization at 200 mV from a prepulse at the indicated voltage. Note that, similar to the result showed in Fig. 4*D*, the two peaks of current in the ON change to one and the kinetics of decay get faster as the prepulse voltage increases. (*F*) Energy barriers produced by the five-state model at three different voltages.

pulse decreased this energy to 17 kJ/mol, but, upon returning to −70 mV, the charge needed to surmount a 27-kJ/mol barrier height to return from B_1 to the A_3 state (Fig. 5*F*). This activation energy difference predicts an A_3-to-B_1 charge movement at 150 mV to be 27 times faster than the B_1-to-A_3 movement at −70 mV. Our results indicate that the difference between the slow kinetic component of the ON (4 ms) is 22 times faster than the slow OFF component (88 ms) (compare Fig. 2*D* with Fig. 4*C*), which is in reasonable agreement with the calculation using the five-state model.

A New H_v1 Channel Kinetic Model Is Needed. Previously, by a fluorophore attached to the S4 voltage sensor in dimeric H_v1 channels, we revealed two S4 charge movements: The first one precedes channel opening, with S4 charge movements in both subunits independently, and the second one correlates with channel opening, defined as the fluorescence hook (18). To make it compatible with our previous model, only B_2 in the present model would be correlated with an open channel. Then, the hook would be the transition from B_2 to B_1, which is fast and closes the channel, while transition B_1 to A_3 would be the main S4 transition, which is slow. In the kinetic model of dimeric H_v1 proposed by us (18), voltage sensor movement involved three closed and one open state, where the movement of both voltage sensors within the dimer is necessary before the opening of the permeation pathway of each subunit (18). Here, we found that each independent H_v1 voltage sensor transits through different states, suggesting that the movement of charge is more complex than previously thought. The most significative fact is that more than 50% of gating charge displacement, on the monomeric H_v1 channel, occurs before opening (in 5 ms at 150 mV, when the open probability of the monomeric H_v1 channel is only 0.2, 65% of the gating charge has been displaced). Dimer formation confers cooperative gating to H_v1 channels (8). Therefore, it is possible that the displacement of dimeric voltage sensors is different from the monomeric voltage sensors movement.

Molecular Mechanism for Trapping. We envision that the rate-limiting step that keeps the charges from returning to their resting configuration involves a blocked-like phenomenon mediated by the arginine side chain, much like the documented blockade of H_v1 channels by guanidinium reagents (31–33). Moreover, as reported before using the dimeric human H_v1 mutant N214R (34, 35) and mouse mutant N210R (24), we found that the N264R mutant open channel behaves as an inward rectifier (*SI Appendix*, Fig. S6). Blockade by the positively charged arginine located in the internal vestibule of the channel should be relieved by hyperpolarizing voltages, and the mutant channel should behave as an inward rectifier as found experimentally (*SI Appendix*, Fig. S6). We should also consider that the mutation introduced at position 264 can decrease proton currents by changing the electrostatic potential in the neighborhood of the H_v1 channel internal entrance. Although our data indicate that the N264 mutant does not modify the channel voltage dependence (*SI Appendix*, Figs. S3 and S4), measurements of this position accessibility to thiol-modifying agents was shown to be state-dependent. However, structural models suggest that this position is outside the electric field (7, 36), but more experiments are needed to confirm this claim. Finally, the inspection of the proton current recording of the monomeric *Ciona*-N264R mutant suggests that the positively charged guanidinium stabilizes the closed state of the channel, making the channel deactivation slower in the dimeric and monomeric *Ciona*-H_v1 (*SI Appendix*, Figs. S3 and S6), and in the dimeric mouse and human H_v1 containing the equivalent N210R (24) and N214R (35) mutation, respectively. A possible explanation to these findings is that the gating charge is trapped when the channel is activated upon depolarization, and it recovers slowly during the repolarization process, as we showed in this study.

We conclude that trapping is a consequence of the presence of the charged arginine chain in position 264. Given the fast deactivation rate shown by the WT monomeric H_v1 channel, the presence of a neutral asparagine in that position may have the effect of collapsing the barrier that separates states A_3 from B_1.

Methods

Mutagenesis, Transcription, and Sequencing. The single N264R mutation was introduced with a QuikChange kit (Promega Corp.) in a pSP64T-contained *C. intestinalis* H_v1 sequence kindly provided by Yasushi Okamura, Osaka University, Osaka, Japan. The ΔNΔC H_v1 was constructed with a stop codon at Val270 and an initiator methionine replacing Glu129 (6). Primers were designed using the web service QuikChange Primer Design. Mutant DNA was amplified by PCR, checked by sequencing, and then linearized with NotI restriction enzyme. In vitro transcription was performed with an mMESSAGE mMACHINE kit (Ambion) using RNA polymerase SP6. RNA was quantified by absorbance at 260 nm, and its integrity was checked by electrophoresis in 1% agarose gel with ethidium bromide at 0.6 μg/μL.

Oocyte Extraction and RNA Injection. *X. laevis* oocytes were obtained and injected with 50 nL of RNA at a concentration of 1 μg/μL according to previously described methodologies (26).

Electrophysiology. Voltage clamp recordings were performed in inside-out giant patches of oocytes membranes (37). The internal and external solutions contained 100 mM Hepes, 2 mM $MgCl_2$, 1 mM EGTA, and 50 mM *N*-methyl-D-glucamine (NMDG)-methanesulfonate. pH was adjusted with NMDG or methanesulphonate to 7.0. Measurements were performed at room temperature (22 °C). Pipettes of borosilicate capillary glass (1B150F-4; World Precision Instruments) were pulled on a horizontal pipette puller (Sutter Instruments) and fire polished until obtaining a diameter between 15 and 24 μm (resistances of 0.8 to 1.2 MΩ in the bath solution). Data were acquired with an Axopatch 200B amplifier (Axon Instruments). Both the voltage command and current output were filtered at 20 kHz with 8-pole Bessel low-pass filters (Frequency Devices). Analog signals were sampled with a 16-bit A/D converter (Digidata 1440A; Axon Instruments) at 250 kHz. Recordings were filtered off-line at 10 kHz by a digital 8-pole Bessel low-pass filter before analysis. Experiments were performed using Clampex 8 acquisition software (Axon Instruments). Capacitive currents were compensated by analog circuitry, and linear capacitive currents were subtracted using a P/-8 protocol with a subsweep holding potential of −90 mV (38).

Gating Current Simulations. A five-state kinetic model was simulated solving the equation $d\boldsymbol{P}(t)/dt = \boldsymbol{P}(t)\mathbf{Q}$, where $\boldsymbol{P}(t)$ is the probability vector of the states and $\boldsymbol{Q}$ is the transition rate matrix. We solved the time dependency of $\boldsymbol{P}(t)$ using the spectral expansion (39). Forward and reverse kinetic constants, $\alpha(V)$ and $\beta(V)$, respectively, were modeled as $\alpha(V) = \alpha_0 \exp(xz\delta e_0 V/kT)$ and $\beta(V) = \beta_0 \exp((x-1)z\delta e_0 V/kT)$, where α_0 and β_0 are the kinetic constants at $V = 0$ mV, $z\delta e_0$ is the charge moved in the transition, x is the fraction of the charge moved from a well to the barrier peak in each forward transition, and k and T have their usual meanings. Gating currents $I_g(t)$ were obtained with the equation $I_g(t) = N\boldsymbol{F}(t)\boldsymbol{Z}$, where N is the number of channels, $\boldsymbol{F}(t)$ is the net occupancy flux of each transition (40), and $\boldsymbol{Z}$ is a vector containing the charge associated to each transition. Parameters used in the model are listed in *SI Appendix*, Table S1.

Note. While this paper was under revision, detection of gating currents in the dimeric human proton channel mutant W207A-N214R (W257A-N264R in *Ciona*-H_v1) was reported (41). The method used by the authors to measure gating currents was stepping to a depolarizing voltage from different holding potentials, which is essentially a "Cole–Moore" protocol. Surprisingly, the gating current data do not show a Cole–Moore effect like the one reported here. This is an unexpected result, considering that the data also indicate that the gating current kinetics is defined by multiple states (41). However, the lack of a well-defined Cole–Moore effect may be due to the fast activation kinetics conferred by the W207A mutation (42).

ACKNOWLEDGMENTS. We thank Dr. David Baez for carrying out some of the initial preliminary experiments. This work was supported by Comisión Nacional de Investigación Científica y Tecnológica (CONICYT)-Programa Formación de Capital Humano Avanzado (PFCHA)/Doctorado Nacional/2017-21170395 (to E.M.C.), Fondo Nacional de Desarrollo Científico y Tecnológico (Fondecyt) Grants ACT 1104, Fondecyt 1180464 (to C.G.), 1150273 (to R.L.), and the US Air Force Office of Scientific Research (AFOSR) under Award FA9550-16-1-0384 (to R.L.). The Centro Interdisciplinario de Neurociencia de Valparaiso is a Millennium Institute supported by the Millennium Scientific Initiative of the Chilean Ministry of Economy, Development, and Tourism (P029-022-F).

1. Sasaki M, Takagi M, Okamura Y (2006) A voltage sensor-domain protein is a voltage-gated proton channel. *Science* 312:589–592.
2. Ramsey IS, Moran MM, Chong JA, Clapham DE (2006) A voltage-gated proton-selective channel lacking the pore domain. *Nature* 440:1213–1216.
3. DeCoursey TE (2018) Voltage and pH sensing by the voltage-gated proton channel, H_V1. *J R Soc Interface* 15:20180108.
4. Lee SY, Letts JA, Mackinnon R (2008) Dimeric subunit stoichiometry of the human voltage-dependent proton channel Hv1. *Proc Natl Acad Sci USA* 105:7692–7695.
5. Tombola F, Ulbrich MH, Isacoff EY (2008) The voltage-gated proton channel Hv1 has two pores, each controlled by one voltage sensor. *Neuron* 58:546–556.
6. Koch HP, et al. (2008) Multimeric nature of voltage-gated proton channels. *Proc Natl Acad Sci USA* 105:9111–9116.
7. Gonzalez C, Rebolledo S, Perez ME, Larsson HP (2013) Molecular mechanism of voltage sensing in voltage-gated proton channels. *J Gen Physiol* 141:275–285.
8. Gonzalez C, Koch HP, Drum BM, Larsson HP (2010) Strong cooperativity between subunits in voltage-gated proton channels. *Nat Struct Mol Biol* 17:51–56.
9. Cherny VV, Markin VS, DeCoursey TE (1995) The voltage-activated hydrogen ion conductance in rat alveolar epithelial cells is determined by the pH gradient. *J Gen Physiol* 105:861–896.
10. Musset B, et al. (2011) Aspartate 112 is the selectivity filter of the human voltage-gated proton channel. *Nature* 480:273–277.
11. Cherny VV, Murphy R, Sokolov V, Levis RA, DeCoursey TE (2003) Properties of single voltage-gated proton channels in human eosinophils estimated by noise analysis and by direct measurement. *J Gen Physiol* 121:615–628.
12. Fujiwara Y, et al. (2012) The cytoplasmic coiled-coil mediates cooperative gating temperature sensitivity in the voltage-gated H(+) channel Hv1. *Nat Commun* 3:816.
13. Larsson HP, Baker OS, Dhillon DS, Isacoff EY (1996) Transmembrane movement of the shaker K+ channel S4. *Neuron* 16:387–397.
14. Mony L, Berger TK, Isacoff EY (2015) A specialized molecular motion opens the Hv1 voltage-gated proton channel. *Nat Struct Mol Biol* 22:283–290.
15. Gandhi CS, Olcese R (2009) The voltage-clamp fluorometry technique. *Potassium Channels: Methods and Protocols*, ed Lippiat JD (Humana, Totowa, NJ), pp 213–231.
16. Cha A, Bezanilla F (1997) Characterizing voltage-dependent conformational changes in the Shaker K+ channel with fluorescence. *Neuron* 19:1127–1140.
17. Mannuzzu LM, Moronne MM, Isacoff EY (1996) Direct physical measure of conformational rearrangement underlying potassium channel gating. *Science* 271:213–216.
18. Qiu F, Rebolledo S, Gonzalez C, Larsson HP (2013) Subunit interactions during cooperative opening of voltage-gated proton channels. *Neuron* 77:288–298.
19. Aggarwal SK, MacKinnon R (1996) Contribution of the S4 segment to gating charge in the Shaker K+ channel. *Neuron* 16:1169–1177.
20. Seoh SA, Sigg D, Papazian DM, Bezanilla F (1996) Voltage-sensing residues in the S2 and S4 segments of the Shaker K+ channel. *Neuron* 16:1159–1167.
21. Baez-Nieto D, et al. (2014) Gating currents of monomeric Hv channel reveals a permeation pathway coupled to the voltage activation. *Biophys J* 106:233a.
22. Carmona EM, et al. (2018) Properties of the voltage-gated proton channel gating currents. *Biophys J* 114(Special Issue 3):546a.
23. De La Rosa V, Ramsey IS (2018) Gating currents in Hv1 proton channels. *Biophys J* 114(Special Issue 3):124a.
24. Sakata S, et al. (2010) Functionality of the voltage-gated proton channel truncated in S4. *Proc Natl Acad Sci USA* 107:2313–2318.
25. Cole KS, Moore JW (1960) Potassium ion current in the squid giant axon: Dynamic characteristic. *Biophys J* 1:1–14.
26. Gonzalez C, Rosenman E, Bezanilla F, Alvarez O, Latorre R (2000) Modulation of the Shaker K(+) channel gating kinetics by the S3-S4 linker. *J Gen Physiol* 115:193–208.
27. DeCoursey TE, Cherny VV (1994) Voltage-activated hydrogen ion currents. *J Membr Biol* 141:203–223.
28. Chandler WK, Rakowski RF, Schneider MF (1976) A non-linear voltage dependent charge movement in frog skeletal muscle. *J Physiol* 254:245–283.
29. Armstrong CM, Bezanilla F (1977) Inactivation of the sodium channel. II. Gating current experiments. *J Gen Physiol* 70:567–590.
30. Bezanilla F, Villalba-Galea CA (2013) The gating charge should not be estimated by fitting a two-state model to a Q-V curve. *J Gen Physiol* 142:575–578.
31. Hong L, Kim IH, Tombola F (2014) Molecular determinants of Hv1 proton channel inhibition by guanidine derivatives. *Proc Natl Acad Sci USA* 111:9971–9976.
32. Hong L, Pathak MM, Kim IH, Ta D, Tombola F (2013) Voltage-sensing domain of voltage-gated proton channel Hv1 shares mechanism of block with pore domains. *Neuron* 77:274–287.
33. Hong L, Singh V, Wulff H, Tombola F (2015) Interrogation of the intersubunit interface of the open Hv1 proton channel with a probe of allosteric coupling. *Sci Rep* 5:14077.
34. Randolph AL, et al. (2016) Proton currents constrain structural models of voltage sensor activation. *eLife* 5:e18017.
35. Ramsey IS, et al. (2010) An aqueous H+ permeation pathway in the voltage-gated proton channel Hv1. *Nat Struct Mol Biol* 17:869–875.
36. Takeshita K, et al. (2014) X-ray crystal structure of voltage-gated proton channel. *Nat Struct Mol Biol* 21:352–357.
37. Hilgemann DW (1995) The giant membrane patch. *Single-Channel Recording*, eds Sakmann B, Neher E (Springer US, Boston), pp 307–327.
38. Armstrong CM, Bezanilla F (1973) Currents related to movement of the gating particles of the sodium channels. *Nature* 242:459–461.
39. Colquhoun D, Hawkes AG (1995) A Q-matrix cookbook. *Single-Channel Recording*, eds Sakmann B, Neher E (Springer US, Boston), pp 589–633.
40. Vandenberg CA, Bezanilla F (1991) A sodium channel gating model based on single channel, macroscopic ionic, and gating currents in the squid giant axon. *Biophys J* 60:1511–1533.
41. De La Rosa V, Ramsey IS (2018) Gating currents in the Hv1 proton channel. *Biophys J* 114:2844–2854.
42. Cherny VV, et al. (2015) Tryptophan 207 is crucial to the unique properties of the human voltage-gated proton channel, hHV1. *J Gen Physiol* 146:343–356.